RSC Advances

PAPER

View Article Online
View Journal | View Issue

Cite this: *RSC Adv.*, 2024, **14**, 83

Highly bright solid-state carbon dots for efficient anticounterfeiting†

Weihua Li,[ab] Yuanyuan Han,[ab] Lihua Wang,[ab] Gurpreet Singh Selopal,[ab] Xiaohan Wang*[ab] and Haiguang Zhao *[ab]

Received 24th October 2023
Accepted 4th December 2023

DOI: 10.1039/d3ra07235e

rsc.li/rsc-advances

Carbon dots (C-dots) as promising fluorescent materials have attracted much attention because of their low toxicity and excellent optoelectronic properties. However, the aggregation-caused quenching (ACQ) of the solid-state C-dots has limited their potential applications in anti-counterfeiting and optoelectronic devices. In this work, C-dot powder was prepared by directly dispersing the as-prepared C-dots in a polymer matrix or *in situ* formation of the C-dot/Ca-complex by vacuum heating in the presence of boric acid. The as-prepared C-dots have high quantum yields (QYs) in the range of 40–67% with temperature-dependent photoluminescent (PL) properties. As a proof of concept, the as-synthesized C-dots were used to produce a flexible anti-counterfeiting code and showed high-level security. This highlights the potential of C-dots in solid-state information, anti-information encryption and anti-counterfeiting.

1. Introduction

Carbon dots (C-dots) are luminescent carbon nanomaterials, which mainly contain carbon, nitrogen, and oxygen,[1,2] and are considered as a building block for a broad range of applications, such as bio-imaging,[3,4] photocatalysis,[5,6] sensing,[7] and anti-counterfeiting.[8,9] There are a variety of anti-counterfeiting strategies, such as quick responsive (QR) codes,[10] labels, ink[11–13] and digital technology.[14,15] In the past few years, C-dots have attracted widespread interest owing to their excellent properties, such as strong luminescence, excellent biocompatibility, long-operation photostability, low cost, low toxicity, and simple synthetic methods.[9,16–18] Although most of the C-dots exhibited potential as fluorescent materials for anti-counterfeiting because of their small particle size and bright emission,[19,20] their emissions were quenched in the solid state due to the aggregation-induced quenching (ACQ), which limits their applications in solid states.[21,22]

To overcome the ACQ issue, there are two strategies for preparing solid-state fluorescent C-dots, which are divided into a two-step method and one-step synthetic method. The two-step method usually involves the post-treatment of the as-prepared C-dots and their capsulation into different matrices, such as polyvinyl alcohol (PVA),[23] silica sol,[24] starch,[25] and polymethyl methacrylate (PMMA).[26] The one-step method generally includes the *in situ* embedding of C-dots,[27,28] surface functionalization,[29–31] aggregation induced luminescence (AIE),[32,33] and regulation of the carbon core.[34,35] For instance, Ai *et al.* reported C-dots with blue to deep red color through surface ligand modulation.[36] The intra- and inter-molecular hydrogen bonding inside the C-dots explained the high quantum yield (QY) of the C-dots in the solid state. Liu *et al.* first prepared C-dots and dispersed them into PVA to fabricate composite films, the emission was much stronger than the control sample.[37] Sun *et al.* chemically dispersed the as-prepared C-dots in SiO_2 networks and obtained effective full-color luminous SiO_2/C-dots composites.[38] To date, it is still a challenge to obtain highly bright solid-state C-dots *via* a simple and low-cost method, and there are no reports of solid-state C-dots applied in anticounterfeiting systems or information encryption.

In this work, highly bright solid-state C-dots were developed for an efficient temperature-sensitive anticounterfeiting system. Several types of C-dot powders were prepared by directly dispersing the as-prepared C-dots in the polymer matrix or *in situ* formation of the C-dots/matrix. The developed C-dot composite exhibited a high QY of 67% and unique temperature-dependent photoluminescence (PL) properties. The as-prepared solid-state C-dot powders were combined with room temperature phosphorescence (RTP) C-dots and used to produce temperature-sensitive flexible anti-counterfeiting codes with high-level security, highlighting the potential prospects of C-dots in the fields of information encryption and anti-counterfeiting.

2. Experimental section

2.1 Materials

Citric acid, urea, boric acid (BA), anhydrous calcium chloride, polyvinyl pyrrolidone (PVP), cyanuric acid (CA), methanol, and ethanol were purchased from Sinopharm Chemical Reagent

[a]*College of Textiles and Clothes, College of Physics, State Key Laboratory of Bio-Fibers and Eco-Textiles, Qingdao University, No. 308 Ningxia Road, Qingdao 266071, P. R. China. E-mail: xh_wang@qdu.edu.cn; hgzhao@qdu.edu.cn*

[b]*Department of Engineering, Faculty of Agriculture, Dalhousie University, Truro, Nova Scotia B2N 5E3, Canada*

† Electronic supplementary information (ESI) available. See DOI: https://doi.org/10.1039/d3ra07235e

Co., Ltd. Distilled water was used in all the experiments. All chemicals were used directly without any purification.

2.2 Synthesis of colloidal C-dots

Colloidal C-dots were synthesized using a vacuum heating approach.[21,39] Specifically, citric acid (1 g), urea (2 g), and $CaCl_2$ (1 g) were mixed with 5 mL water. The obtained solution was directly heated to 200 °C or 250 °C under vacuum. These temperatures were maintained for 2 hours to obtain the C-dot powder. The as-prepared powder was dispersed in methanol and the supernatant was collected by centrifugation. The C-dots synthesized at 200 °C and 250 °C were denoted as C-dots (200 °C) and C-dots (250 °C), respectively.

2.3 Synthesis of RTP C-dots

RTP C-dots were synthesized using a vacuum heating approach.[40] Specifically, 1 g of ethylenediamine and 3 g of phosphoric acid were dissolved in deionized water (4 g). The mixture was heated to 250 °C under vacuum and maintained at this temperature for 5 h. Once the flask was cooled down to 25 °C, the solid powder was dispersed in water and centrifuged at 8000 rpm for 10 min. After dialysis, the mixture was freeze-dried to obtain the RTP powder.

2.4 Preparation of C-dots embedded in different matrices

C-dots@PVP. The as-prepared C-dots (200 °C) or C-dots (250 °C) were mixed with the PVP polymer in a weight ratio of 1 : 100, and further dissolved in ethanol. The obtained clear mixture was dried in a vacuum drying furnace at 80 °C for 12 h. The obtained powder was grounded using agate mortar. The composites prepared using C-dots (250 °C) or C-dots (200 °C) were demoted as C-dots@PVP and C-dots@PVP (200 °C).

C-dots@CA. Ten milligrams of C-dots (250 °C) powder was dispersed in water (100 °C, 200 mL) and one gram of cyanic acid was added to the above mixture. After heating the mixture for 1 hour, the mixture was cooled down to 20 °C and the obtained powder was used for further characterization. The as-obtained powder was denoted as C-dots@CA.

C-dots/BNO. For the direct production of the C-dots/matrix, the mixture of citric acid, urea, BA, and $CaCl_2$ was mixed with water and heated to 250 °C for 1 hour under vacuum. The weight ratios of the citric acid, urea, CaC_{l2}, and BA were 1 : 2 : 1 : 0.5. The concentration of the citric acid was 0.2 g mL^{-1}. The as-obtained powder was purified using ethanol. The yellow precipitate was collected and freeze-dried for further characterization. The powder prepared in this approach was denoted as C-dots@BNO.

2.5 Security code preparation

C-dots@PVP, C-dots@BNO, and RTP C-dot powder were directly dispersed in ethanol to form a fluorescent ink, and then the designed pattern was handwritten on non-fluorescent paper.

2.6 Characterization

Transmission electron microscopy (TEM) and high-resolution TEM (HRTEM) studies on C-dots were performed using a JEOL 2100F TEM. C-dot composites were analyzed using the Zeiss Gemini field emission scanning electron microscope (SEM) coupled with energy dispersive spectroscopy (EDS). A Thermo Scientific K-Alpha photoelectron spectrometer was used to measure the X-ray photoelectron spectroscopy (XPS) of C-dots. The steady-state and transient PL spectra of C-dots were characterized using an Edinburgh FLS1000 instrument. The QYs of the C-dots were measured using a Hamamatsu QY measurement system C9920-02G integrated with an integrating sphere. The QY was calculated using the equation: QY = the emitted photons/the absorbed photons, where the number of emitted photons and absorbed photons were calculated from the data in Fig. 4c. Ultraviolet (UV)-visible (Vis) absorption spectra of the C-dots were collected on a Lambda 750 UV/VIS spectrometer (PerkinElmer). The magnetic agitator ZNCL-BS was used for heating and a high accuracy portable thermocouple thermometer YET-610 was used for temperature measurements. Light-emitting diodes (LEDs) with wavelengths of 365 nm and 395 nm were used to excite the samples with a typical powder intensity of 5 W cm^{-2}.

3. Results and discussion

3.1 Synthesis and structure of C-dots

To obtain solid-state C-dots, two approaches were used in this work. For the first method, the C-dots were first synthesized *via* a vacuum heating approach and then embedded in matrices (Fig. 1a). For the second method, we added BA to the reaction system (citric acid/urea and $CaCl_2$) to form C-dot composite through dehydration and crosslinking reaction (Fig. 1b). We could obtain a bright green powder *via* a one-step reaction (second method). The reaction details are included in the Experimental section. The obtained C-dots appeared as a slightly yellow powder and emitted bright green PL upon UV (395 nm) illumination (Fig. 1c and d) for the C-dot composite. After 10 h illumination, the C-dots maintained 95%, 87%, 73%, and 95% of its initial value, indicating that it has good photostability (Fig. S1†).

The morphologies and structures of the as-prepared C-dots were characterized by TEM and SEM. The as-prepared C-dots (250 °C) have a quasi-spherical shape with a mean size of 5–6 nm (Fig. 2a). HRTEM further revealed the *d*-spacing of 0.22 nm for C-dots (Fig. S2†), attributed to the (100) facets of graphite.[39] We further performed dynamic light scattering (DLS) measurements on the C-dot solution, which showed that the particle size was mainly distributed at ~8 nm (Fig. S3†). Fig. 2b–e shows the SEM micrographs of C-dot@PVP, C-dots@CA, C-dots@BNO, and C-dots@PVP (200 °C), respectively. We were not able to observe the C-dots inside the matrix, but we observed significant differences between the C-dots/PVP polymer and C-dots/BNO or C-dots/CA. A honeycomb structure was found for the C-dots/CA and C-dots/BNO, which might be due to the evaporation of the solvent at high temperatures. EDS confirmed that all the samples had C/N/O, as shown in Fig. 2f. The presence of Ca and Cl is due to the formation of the Ca-complex, NH_4Cl, and $CaCl_2$, consistent with the XPS results.

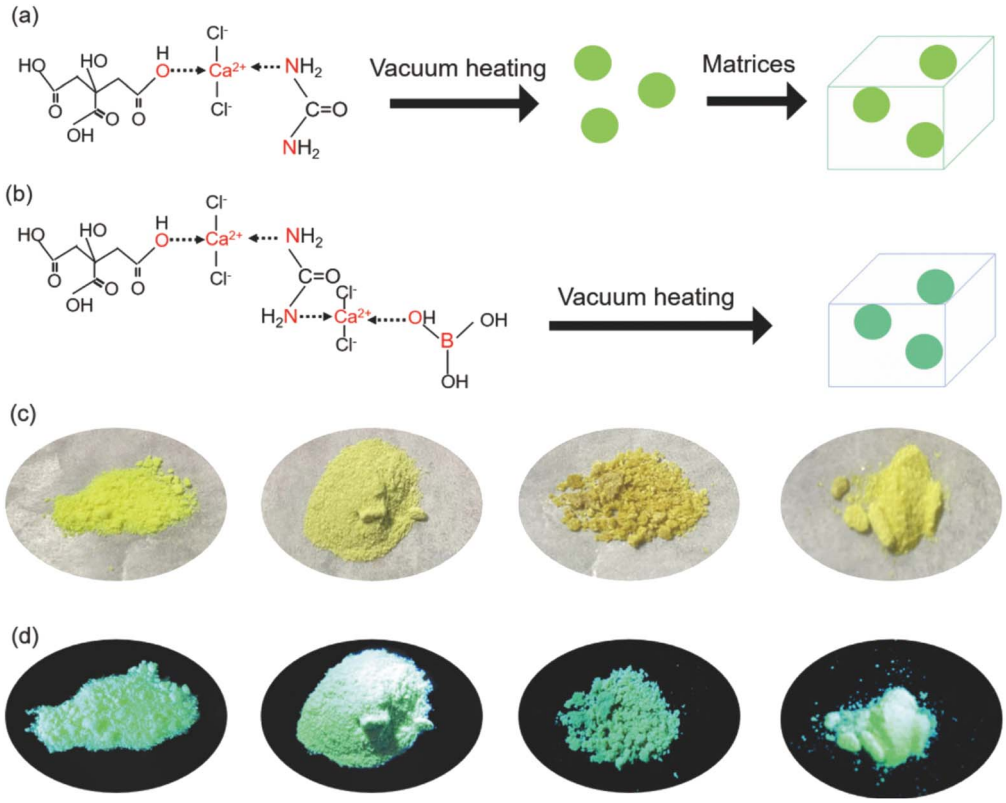

Fig. 1 (a) Schematic illustration for the two-step synthesis progress of C-dot@PVP, C-dot@CA, and C-dot@PVP (200 °C). (b) Schematic illustration for the one-step synthesis progress of C-dot@BNO. (c and d) Images of different C-dot composites under (c) daylight and (d) UV illumination (λ_{ex} = 395 nm). From left to right, the C-dot composites are C-dots@PVP, C-dots@CA, C-dots@BNO, and C-dots@PVP (200 °C), respectively.

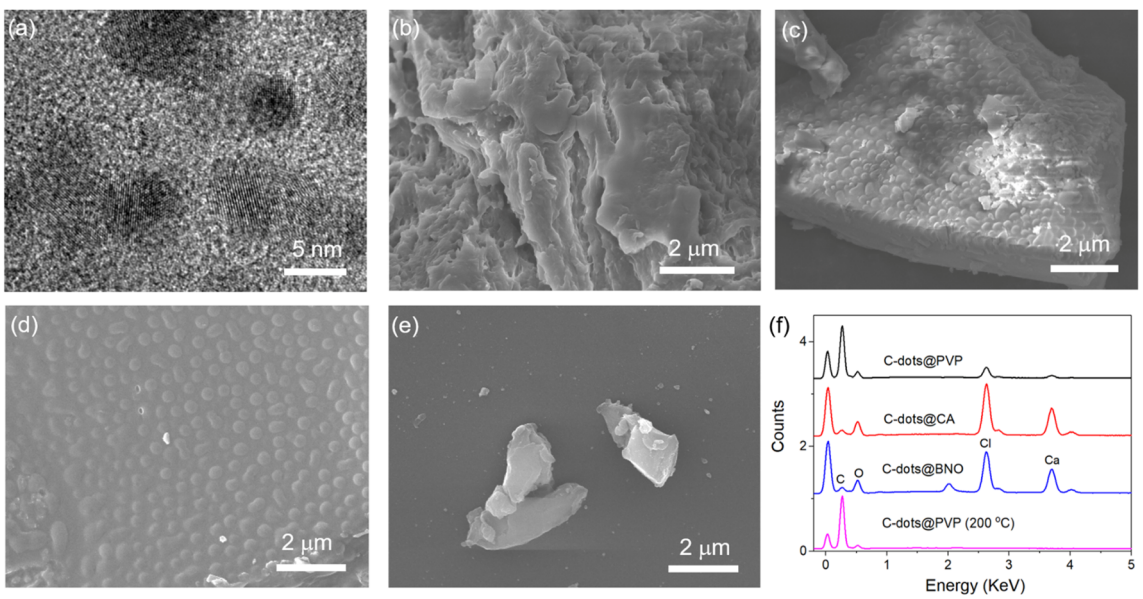

Fig. 2 (a) HRTEM images of C-dots synthesized at 250 °C. (b–e) SEM images of (b) C-dots@PVP, (c) C-dots@CA, (d) C-dots@BNO, and (e) C-dots@PVP (200 °C); (f) EDS of the C-dot composites.

To further explore the surface composition of C-dots, the high-resolution XPS spectra of the C-dots@PVP, C-dots@BNO and C-dots@CA, C-dots@PVP (200 °C), and C-dots (250 °C) were recorded and analyzed. The survey spectra of XPS demonstrated that the as-prepared C-dots@PVP were mainly composed of C, N, O, Ca, and Cl elements and the C-dots@BNO contains C, N, O, Ca,

Cl, and B elements (Fig. S4c†). As shown in Fig. 3a, the high-resolution C 1s spectra of the four C-dots were fitted into four peaks at 284.8 eV, 285.7 eV, 287.5 eV, and 288.9 eV, which correspond to C=C/C–C, C–N, C–O, and C=O,[41–43] respectively. The N 1s spectra of C-dots can be fitted into two peaks at 399.7 eV and 401.3 eV, assigned to pyridinic N and the amine N (Fig. 3b).[44,45] Peaks for C–O (532.7 eV) and C=O (531.4 eV) were present in O 1s high-resolution spectra (Fig. 3c).[46] For C-dots@BNO, the broad B 1s spectrum can be fitted by a main peak (192.4 eV), which is due to B–N/B–O bonds (Fig. 3d).[31,39] It revealed that boron atoms reacted with N and O atoms on the carbonaceous structure of the C-dots to form the BNO complex. Based on XPS results, C-dots/CA and C-dots/BNO exhibited a stronger interaction between C-dots and matrices than with PVP. This phenomenon is also reflected in the solubility of the composites. C-dots/PVP can be dispersed easily in ethanol and water, while C-dots/CA and C-dots/BNO could not be dispersed in ethanol and water at room temperature due to their different surrounding matrixes.

3.2 Optical properties of the C-dot composite

As shown in Fig. 4, the UV-visible spectra of the C-dots in the solution and powder were recorded. The C-dots dispersed in ethanol exhibited two peaks, centered at 330 nm and 405 nm (Fig. 4a). Typically, the peak of 405 nm originated from the n–π* transition of aromatic sp^2 system containing the C=O bond,[47] and the strong absorption peak at 330 nm is due to the n–π* transition of the conjugate C=O/C=N.[39,47] When the heating temperature increases from 200 °C to 250 °C, the ratio of the absorption peak intensities at 330 nm and 405 nm decreases, indicating that the content of the aromatic carbon (sp^2 C) increases under the reaction condition of 250 °C.[47] As shown in Fig. 4b, the solid-state C-dot composite shows obvious absorption peaks at 250–260 nm, which is attributed to the π–π* electron transition of aromatic C=C.[48,49] For C-dots@BNO, the absorption peak at about 300 nm disappeared, indicating that the formation of the composite is accompanied by the destruction of the C=O bond and formation of a new surface emission state.[31]

We further measured the QYs of the four types of C-dots. QYs of C-dots@PVP, C-dots@CA, C-dots@BNO, and C-dots@PVP (200 °C) are 67%, 28%, 45%, and 40%, respectively (Fig. 4c). Notably, the QY value of C-dots@PVP and C-dots@BNO is very similar to the QY of the liquid C-dots (250 °C) and boron-doped C-dots (69.8% and 41.1%) (Fig. S5†), indicating that the efficient encapsulation of C-dots by matrices. As shown in Fig. S6,† the as-prepared C-dot powders have lifetimes of 10 ns (C-dots@PVP), 9.7 ns (C-dots@CA), 10 ns (C-dots@BNO), and 12.6 ns (C-dots@PVP (200 °C)). The decrease of QY from 67% to 28% for the C-dots (250 °C) before and after being embedded in CA might be due to the newly created surface traps/defects during the heating process at 100 °C. The increase of the QY from 17.6% to 40% for the C-dots (200 °C) after embedding in PVP could be due to the improved surface passivation as also evidenced by their unchanged PL peak as a function of excitation wavelengths compared to the strong excitation-dependent PL peaks for the liquid-state C-dots (Fig. S7a and f†).

Compared to the C-dots produced at 200 °C, the C-dots (250 °C) have a less PL shift as a function of the excitation wavelength, indicating that higher reaction temperature leads to a stable energy state. The C-dot composite has excitation-independent emissions, which indicates that the encapsulating matrix stabilizes the energy states (Fig. S7c–f†). We further measured the PL intensity of four types of C-dot composites at different temperatures in the range of 30 °C to 150 °C. As shown in Fig. 5a–d, all C-dots exhibited a temperature-dependent PL behavior, in which the PL intensity decreased with increasing temperature, and the decrease may be attributed to the enhanced non-radiative recombination with the increase in temperature. This is due to heat-activated non-radiative capture as reported previously for the C-dots.[50,51] Non-radiative channels, including defect states and ionized impurity states, are activated at higher temperatures and provide more opportunities for the excited electrons to return to the ground state through non-radiative processes, resulting in a reduction in fluorescence intensity.[52–54] The C-dots (250 °C)@PVP maintained 89% of its initial intensity, which is higher than that of other composites (67% of C-dots/CA; 72% of C-dots/BNO and 72% of C-dots (200 °C)@PVP) (Fig. 5). In other words, C-dots with higher QY showed a less decrease in the PL intensity with the increase of temperature. This is because the C-dots with high QY have fewer surface defects and the surface thermal-activated vibration of C-dots is inhibited.[31]

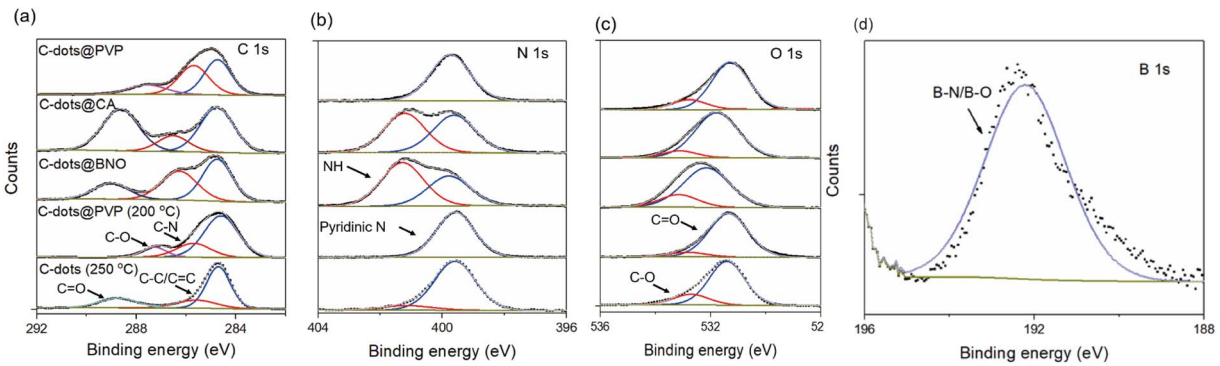

Fig. 3 High-resolution XPS spectra of (a) C 1s, (b) N 1s, (c) O 1s, and (d) B 1s of the C-dots@PVP, C-dots@CA, C-dots@BNO, C-dots@PVP (200 °C), and C-dots (250 °C).

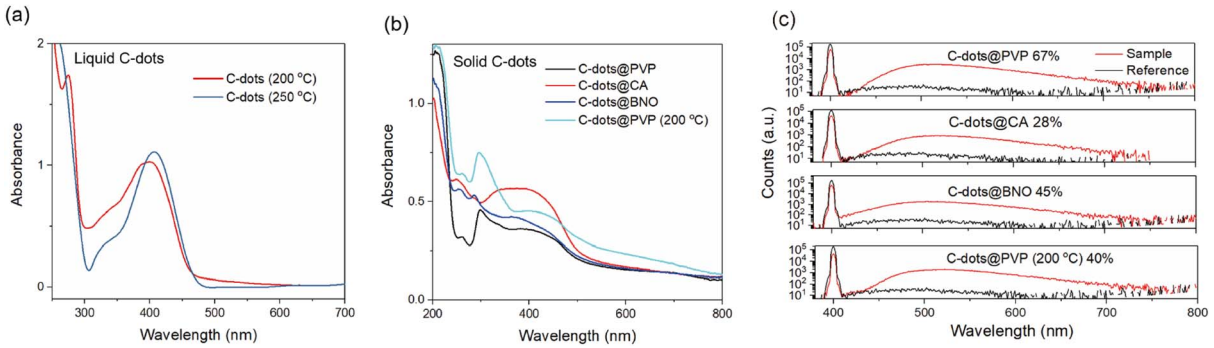

Fig. 4 (a) Absorption spectra of C-dots (200 °C) and C-dots (250 °C) dispersed in ethanol; (b) absorption spectra of C-dots@PVP, C-dots@CA, C-dots@BNO, and C-dots@PVP (200 °C). (c) QYs of the C-dots@PVP, C-dots@CA, C-dots@BNO, and C-dots@PVP (200 °C).

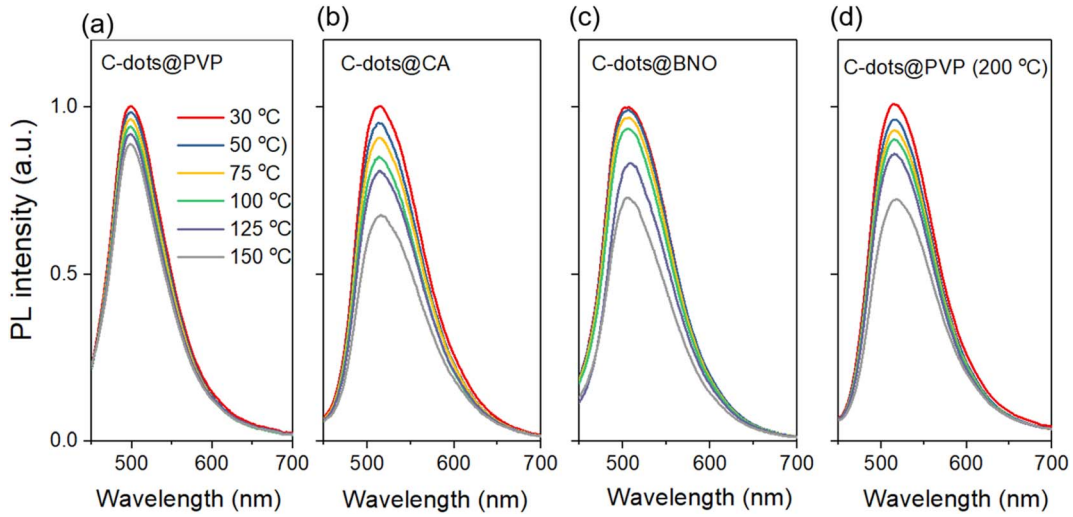

Fig. 5 PL spectra of the C-dot composites measured at the temperature range of 30 °C to 150 °C: (a), C-dots@PVP (b) C-dots@CA, (c) C-dots@BNO, and (d) C-dots@PVP (200 °C).

3.3 Anticounterfeiting applications of the C-dot composites

Considering the unique temperature response properties, the C-dots showed great potential in anti-counterfeiting, information security, and other applications. As a proof of concept, we selected the C-dots@PVP and C-dots@BNO with different temperature-sensitive behaviors for security code fabrication. As shown in the pattern "888" (Fig. 6a), the sample C-dots@BNO was used in the green part, C-dots@PVP was used in the light-yellow part, and PVP was used in the gray part. The code was written on the non-fluorescent Daolin paper with a brush and displayed a light white "888" in daylight at room temperature, while the number 886 with green fluorescence was observed upon illumination with light (395 nm) under different temperatures of 30–150 °C (Fig. 6a).

We measured the PL spectra of C-dots@PVP and C-dots@BNO in the printed pattern with temperature change using a homemade PL detector with an accurate detected area of 2×4 mm^2. This setup enables the detection of the code with the area pointed by C-dots@PVP (green part) or C-dots@BNO (yellow part). As shown in Fig. 6c and d, the emission peak position of both types of the C-dot composites after printing was basically unchanged. However, the PL intensity of the C-dot composite (detected area of 2×4 mm^2) strongly decreased with the increase of the temperature from 30 °C to 150 °C (Fig. 6c and d). We analyzed the brightness of the C-dot composite located at the green or yellow part of the code using PL spectra. A different decrease rate as a function of temperature leads to different PL integrated areas between the two detected regions (Fig. 6e) and this temperature-sensitive radiometric PL code strongly improved the security level of the code. Meanwhile, by the combination of the C-dots/PVP powder and RTP C-dot powder, we produced the code "888". Without seeing any color at room light, we can see clearly the 888 upon illumination with 365 nm light. After switching off the UV light, a clear RTP code of "111" showed up and lasted for 2 seconds with a yellow-green shape (Fig. 6b), indicating that the as-prepared fluorescent powder could combine with the RTP C-dot system for multiple and high-level optical security.

In addition, C-dot composite has great promise in fingerprint visualization detection technology,[55] as shown in

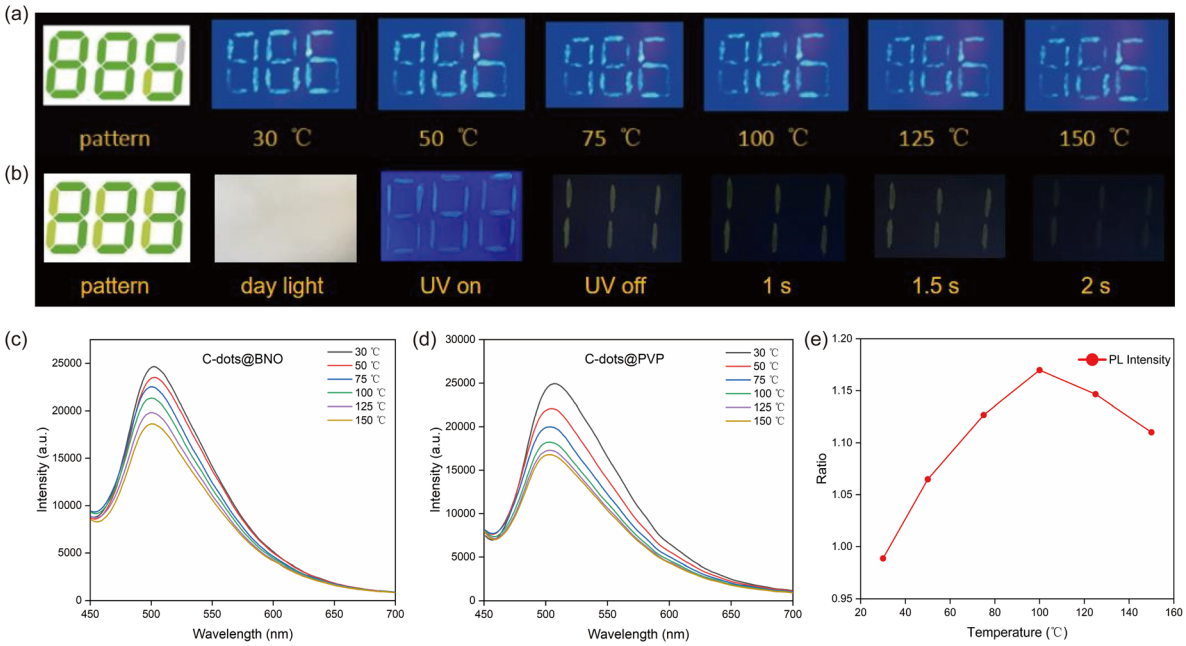

Fig. 6 (a) Design and fluorescence images of the anti-counterfeiting patterns "888" at different temperatures (λ_{ex} = 395 nm), C-dots@PVP for the green part, C-dots@BNO for the light-yellow part, and PVP for the gray part. (b) Patterns "888" under room light, 395 nm UV light, and after switching off the UV light. PL spectra of the (c) C-dots@PVP and (d) C-dots@BNO based code at different temperatures (λ_{ex} = 365 nm). (e) Integrated PL intensity ratio between C-dots@PVP and C-dots@BNO at different temperatures.

Fig. S9a.† We used the C-dots@PVP fluorescent ink to press the fingerprint on non-fluorescent Daolin paper, which is not visible in daylight but can be clearly seen when illuminated with a UV lamp. We can also utilize the excitation dependence PL properties of the C-dots to achieve multiple security codes (Fig. S9b†). The number "888" was invisible under daylight, and patterns of different colors appeared when different wavelengths of UV light were used.

To avoid the decrease of PL and RTP properties after printing, the polymer film was used to seal the code, which can significantly block the influence from the surrounding environments. This post-treatment does not affect the flexibility of the substrate, but greatly improves the long-term stability of the security code. There was no significant variation after three months of storage at ambient conditions.

4. Conclusions

In conclusion, we demonstrated several types of solid-state C-dot composites prepared *via* one-step or two-step approaches for high-level temperature-sensitive security codes. The as-prepared C-dot composites showed a bright green color with QYs of as high as 67% in the solid-state benefiting from the isolation of the C-dots by the matrix to prohibit the ACQ. The as-prepared C-dot composites exhibited a strong temperature-dependent PL behavior. As these powders have also different QYs, we can easily design and prepare the fluorescent code for the anticounterfeiting system. As a proof-of-concept, we designed and prepared a ratio-metric PL and PL/RTP security code with a high-security level and excellent long-term operation stability. The flexible anti-counterfeiting code can be potentially used for high-level information encryption and anti-counterfeiting and other solid-state lighting devices, such as luminescent solar concentrators and LEDs.

Conflicts of interest

There are no conflicts to declare.

Acknowledgements

H. Zhao thanks the funding support from the Youth Innovation Team Project of Shandong Provincial Education Department. X. Wang thanks the funding support from Shandong Natural Science Funds (ZR2022EQ036). G. S. S. acknowledges the DAL-AC for the financial support and NSERC Discovery Grant.

Notes and references

1 B. Wang and S. Lu, *Matter*, 2022, **5**, 110–149.
2 J. Yu, H. Song, X. Li, L. Tang, Z. Tang, B. Yang and S. Lu, *Adv. Funct. Mater.*, 2021, **31**, 2107196.
3 P. Li, S. Liu, X. Yang, S. Du, W. Tang, W. Cao, J. Zhou, X. Gong and X. Xing, *Chem. Eng. J.*, 2021, **403**, 126387.
4 B. B. Karakoçak, A. Laradji, T. Primeau, M. Y. Berezin, S. Li and N. Ravi, *ACS Appl. Mater. Interfaces*, 2021, **13**, 277–286.
5 Y. Yao, H. Zhang, K. Hu, G. Nie, Y. Yang, Y. Wang, X. Duan and S. Wang, *J. Environ. Chem. Eng.*, 2022, **10**, 107336.
6 J. Wang, J. Jiang, F. Li, J. Zou, K. Xiang, H. Wang, Y. Li and X. Li, *Green Chem.*, 2023, **25**, 32–58.
7 J. Zhang and S.-H. Yu, *Mater. Today*, 2016, **19**, 382–393.

8 S. Ren, B. Liu, M. Wang, G. Han, H. Zhao and Y. Zhang, *J. Mater. Chem. C*, 2022, **10**, 11338–11346.
9 S. Kalytchuk, Y. Wang, K. Poláková and R. Zbořil, *ACS Appl. Mater. Interfaces*, 2018, **10**, 29902–29908.
10 A. Abdollahi, B. Ghasemi, S. Nikzaban, N. Sardari, S. Jorjeisi and A. Dashti, *ACS Appl. Mater. Interfaces*, 2023, **15**, 7466–7484.
11 A. Abdollahi, H. Roghani-Mamaqani, B. Razavi and M. Salami-Kalajahi, *ACS Nano*, 2020, **14**, 14417–14492.
12 A. Abdollahi, K. Sahandi-Zangabad and H. Roghani-Mamaqani, *ACS Appl. Mater. Interfaces*, 2018, **10**, 39279–39292.
13 A. Abdollahi, N. Hanaei, M. Rahmanidoust and A. Dashti, *J. Colloid Interface Sci.*, 2023, **630**, 242–256.
14 A. T. Mogharbel, S. O. Alzahrani, M. M. Abualnaja, A. M. Albonayan, A. R. Z. Almotairy, H. M. Abumelha and N. M. El-Metwaly, *Ceram. Int.*, 2023, **49**, 27060–27068.
15 R. T. Mogharbel, A. Almahri, O. Alaysuy, S. O. Alzahrani, A. Q. Alorabi, S. D. Al-Qahtani and N. M. El-Metwaly, *Opt. Mater.*, 2023, **141**, 113936.
16 J. Li and X. Gong, *Small*, 2022, **18**, 2205099.
17 H. Zhao, G. Liu, S. You, F. V. A. Camargo, M. Zavelani-Rossi, X. Wang, C. Sun, B. Liu, Y. Zhang, G. Han, A. Vomiero and X. Gong, *Energy Environ. Sci.*, 2021, **14**, 396–406.
18 C.-F. Wang, R. Cheng, W.-Q. Ji, K. Ma, L. Ling and S. Chen, *ACS Appl. Mater. Interfaces*, 2018, **10**, 39205–39213.
19 H. Alharbi, N. A. Alenazi, A. R. Z. Almotairy, S. Sallam, K. Alkhamis, K. F. Alshammari and N. M. El-Metwaly, *J. Inorg. Organomet. Polym.*, 2023, **33**, 3293–3303.
20 S. D. Al-Qahtani, Z. Osama Owidah, A. M. Al-bonayan, M. M. Abualnaja, K. M. Alkhamis, S. H. Alrefaee and N. M. El-Metwaly, *J. Photochem. Photobiol., A*, 2023, **443**, 114833.
21 D. Zhou, P. Jing, Y. Wang, Y. Zhai, D. Li, Y. Xiong, A. V. Baranov, S. Qu and A. L. Rogach, *Nanoscale Horiz.*, 2019, **4**, 388–395.
22 J. Wang, Q. Li, J. Zheng, Y. Yang, X. Liu and B. Xu, *ACS Sustainable Chem. Eng.*, 2021, **9**, 2224–2236.
23 K. Zheng, X. Li, M. Chen, Y. Gong, A. Tang, Z. Wang, Z. Wei, L. Guan and F. Teng, *Chem. Eng. J.*, 2020, **380**, 122503.
24 T. Sarkar, K. Rawat, P. R. Solanki and H. B. Bohidar, *Colloids Surf., A*, 2019, **583**, 123844.
25 Y. Yan, L. Yin, H. Guo, L. Wang and J. Zhang, *IEEE Photonics J.*, 2022, **14**, 1–6.
26 Z. Wei, B. Wang, M. Xie, D. Hong, X. Yang, S. Wan, W. Yang, S. Lu and Y. Tian, *Chin. Chem. Lett.*, 2022, **33**, 751–756.
27 C.-L. Shen, J.-H. Zang, Q. Lou, L.-X. Su, Z. Li, Z.-Y. Liu, L. Dong and C.-X. Shan, *Carbon*, 2018, **136**, 359–368.
28 J. Su, S. Lu, J. Hai, K. Liang, T. Li, S. Sun, F. Chen, Z. Yang and B. Wang, *ACS Sustain. Chem. Eng.*, 2020, **8**, 17687–17696.
29 J. Zheng, Y. Wang, F. Zhang, Y. Yang, X. Liu, K. Guo, H. Wang and B. Xu, *J. Mater. Chem. C*, 2017, **5**, 8105–8111.
30 F. Yan, H. Zhang, J. Xu, Y. Wu, Y. Zang and J. Sun, *ACS Sustainable Chem. Eng.*, 2021, **9**, 3901–3908.
31 H. Wang, Z. Zhang, Q. Yan, C. Zhang, Y. Xing, Y. Xiong, F. Zhang and Z. Wang, *ChemistrySelect*, 2020, **5**, 13969–13973.
32 R. Guo, T. Li and S. Shi, *J. Mater. Chem. C*, 2019, **7**, 5148–5154.
33 H. Yang, Y. Liu, Z. Guo, B. Lei, J. Zhuang, X. Zhang, Z. Liu and C. Hu, *Nat. Commun.*, 2019, **10**, 1789.
34 H. Li, Z. Zhang, J. Ding, Y. Xu, G. Chen, J. Liu, L. Zhao, N. Huang, Z. He, Y. Li and L. Ding, *Carbon*, 2019, **149**, 342–349.
35 Y. Choi, B. Kang, J. Lee, S. Kim, G. T. Kim, H. Kang, B. R. Lee, H. Kim, S.-H. Shim, G. Lee, O.-H. Kwon and B.-S. Kim, *Chem. Mater.*, 2016, **28**, 6840–6847.
36 L. Ai, Z. Song, M. Nie, J. Yu, F. Liu, H. Song, B. Zhang, G. I. N. Waterhouse and S. Lu, *Angew. Chem., Int. Ed.*, 2023, **62**, e202217822.
37 Y. Liu, P. Wang, K. A. Shiral Fernando, G. E. LeCroy, H. Maimaiti, B. A. Harruff-Miller, W. K. Lewis, C. E. Bunker, Z.-L. Hou and Y.-P. Sun, *J. Mater. Chem. C*, 2016, **4**, 6967–6974.
38 M. Sun, Y. Han, X. Yuan, P. Jing, L. Zhang, J. Zhao and Y. Zheng, *Nanoscale*, 2020, **12**, 15823–15831.
39 S. Ren, B. Liu, G. Han, H. Zhao and Y. Zhang, *Nanoscale*, 2021, **13**, 12149–12156.
40 X. Wang, Y. Han, W. Li, J. Li, S. Ren, M. Wang, G. Han, J. Yu, Y. Zhang and H. Zhao, *Adv. Opt. Mater.*, 2023, 2301962.
41 S. D. Dsouza, M. Buerkle, P. Brunet, C. Maddi, D. B. Padmanaban, A. Morelli, A. F. Payam, P. Maguire, D. Mariotti and V. Svrcek, *Carbon*, 2021, **183**, 1–11.
42 X. Miao, D. Qu, D. Yang, B. Nie, Y. Zhao, H. Fan and Z. Sun, *Adv. Mater.*, 2018, **30**, 1704740.
43 J. Guo, Y. Lu, A.-Q. Xie, G. Li, Z.-B. Liang, C.-F. Wang, X. Yang and S. Chen, *Adv. Funct. Mater.*, 2022, **32**, 2110393.
44 H. A. Nguyen, I. Srivastava, D. Pan and M. Gruebele, *ACS Nano*, 2020, **14**, 6127–6137.
45 J. Guo, H. Li, L. Ling, G. Li, R. Cheng, X. Lu, A.-Q. Xie, Q. Li, C.-F. Wang and S. Chen, *ACS Sustain. Chem. Eng.*, 2020, **8**, 1566–1572.
46 J. Tan, R. Zou, J. Zhang, W. Li, L. Zhang and D. Yue, *Nanoscale*, 2016, **8**, 4742–4747.
47 X. Liu, H. Jiang, J. Ye, C. Zhao, S. Gao, C. Wu, C. Li, J. Li and X. Wang, *Adv. Funct. Mater.*, 2016, **26**, 8694–8706.
48 C. Xia, S. Zhu, T. Feng, M. Yang and B. Yang, *Adv. Sci.*, 2019, **6**, 1901316.
49 H. Xu, L. Yan, V. Nguyen, Y. Yu and Y. Xu, *Appl. Surf. Sci.*, 2017, **414**, 238–243.
50 T. Xiao, Y. Li, T. Wang, Y. Fan, F. He, Q. Wang, J. Han, Z. Yin, Z. Yang, J. Qiu and Z. Song, *Mater. Chem. Front.*, 2021, **5**, 4280–4290.
51 Y. Jiang, X. Zhang, L. Xiao, R. Yan, J. Xin, C. Yin, Y. Jia, Y. Zhao, C. Xiao, Z. Zhang and W. Song, *Carbon*, 2020, **163**, 26–33.
52 P. Yu, X. Wen, Y.-R. Toh and J. Tang, *J. Phys. Chem. C*, 2012, **116**, 25552–25557.
53 Z. Mu, J. Hua and Y. Yang, *Spectrochim. Acta, Part A*, 2020, **224**, 117444.
54 S. Kalytchuk, K. Poláková, Y. Wang, J. P. Froning, K. Cepe, A. L. Rogach and R. Zbořil, *ACS Nano*, 2017, **11**, 1432–1442.
55 A. Abdollahi, A. Dashti, M. Rahmanidoust and N. Hanaei, *Sens. Actuators, B*, 2022, **372**, 132649.